nature chemistry

ARTICLES

https://doi.org/10.1038/s41557-018-0066-z

Solvents can control solute molecular identity

Devon. R. Widmer* and Benjamin J. Schwartz*

For solution-phase chemical reactions, the solvent is often considered simply as a medium to allow the reactants to encounter each other by diffusion. Although examples of direct solvent effects on molecular solutes exist, such as the compression of solute bonding electrons due to Pauli repulsion interactions, the solvent is not usually considered a part of the chemical species of interest. We show, using quantum simulations of Na_2, that when there are local specific interactions between a solute and solvent that are energetically on the same order as a hydrogen bond, the solvent controls not only the bond dynamics but also the chemical identity of the solute. In tetrahydrofuran, dative bonding interactions between the solvent and Na atoms lead to unique coordination states that must cross a free energy barrier of ~8 k_BT—undergoing a chemical reaction—to interconvert. Each coordination state has its own dynamics and spectroscopic signatures, highlighting the importance of considering the solvent in the identity of condensed-phase chemical systems.

Although most chemical reactions take place in solution, the solvent is usually thought of as a spectator, acting merely as a medium to hold the reactants and allow them to encounter each other by diffusion. Of course, for a few special cases, such as solvated electrons[1] and the charge-transfer-to-solvent transitions[2] of simple anions, the solvent creates the electronic states that are of importance, primarily because the electrons of interest are not otherwise bound without the stabilizing presence of the solvent. Moreover, in electron transfer and related reactions, reorganization of the surrounding solvent molecules is the driving force to move the electron from the donor to the acceptor, and thus determines the reaction rate[3–5]. Dielectric effects from collective solvent motions can lead to solvatochromic shifts in the electronic absorption spectra of solutes[6], and solvent molecules can provide viscous drag that changes the dynamics and thus the branching ratios of unimolecular isomerization reactions[7]. In terms of more direct solvent effects on molecular solutes, in previous work we have shown that Pauli repulsion interactions from the electrons on the first-shell solvent molecules can compress a solute's bonding electrons, pushing the solute's electron density off axis and raising the bond's vibrational frequency[8]. However, even with these wide-ranging ways in which solvents can affect chemical reactivity, in none of these cases is the solvent thought of as being a part of the chemical species of interest.

In this Article we show, using mixed quantum/classical (MQC) molecular dynamics (MD) simulations, that local specific interactions between a solute and solvent that are energetically on the same order as a hydrogen bond not only alter solute molecular properties but also play an important role as part of the molecular identity of the solute. By simulating the sodium dimer (Na_2) molecule in both liquid Ar and liquid tetrahydrofuran (THF), we show that Pauli repulsion interactions between the solvent molecules and the solute bonding electrons deform the Na_2 bonding electron density. This induces large dipole moments and creates infrared activity in what in the gas phase is a symmetric diatomic solute with no infrared absorption. In liquid THF, dative bonding interactions between the THF oxygen atoms and the sodium cation core at the centre of each Na atom create a series of distinct, chelated solvation states, causing even further distortion of the bonding electrons and, in some cases, the induction of permanent dipole moments. Furthermore, we find that distinct local THF solvation states each have their own unique Na–Na bond length, bond frequency, dynamics and spectroscopic signatures, and that these different chelation states are separated by barriers of many k_BT in free energy. Thus, to explain the behaviour of Na_2 in liquid THF, the different chelated solvation states, which are distinguished only by the weak solute–solvent dative bonds, must be treated as distinct chemical species.

We chose to study the Na_2 molecule in this work because it can be well described in MQC MD simulations. The molecule can be thought of as two classical Na^+ cores that are held together by two quantum mechanical valence bonding electrons[8]. In our simulations, we treat the two quantum mechanical bonding electrons using configuration-interaction-with-singles-and-doubles (CISD)[9], which is equivalent to full configuration interaction because only two explicit electrons are involved. The interactions between the bonding electrons and the Na^+ cores[10] and the THF[11–13] or Ar[14] solvent molecules are described using previously developed pseudopotentials[15]. In this way, we can accurately calculate how immersion of Na_2 in solvents like liquid Ar or THF affects the molecular electronic and vibrational structure of this relatively simple solute. Details of the potentials and computational methods we use are provided in Supplementary Section 'Mixed Quantum/Classical Model' but in general are similar to those in our previous work[8,9,13]. We note that we used these same potentials and level of theory to simulate the structure, spectroscopy and excited-state dynamics of the sodium anion (Na^-) in liquid THF, and obtained excellent agreement with experiment[10,12]. The Na_2/THF system studied here is theoretically identical to our previously studied Na^-/THF system except for the presence of a second identically theoretically treated sodium nucleus.

Results and discussion

Because there is relatively little exchange and correlation between the bonding electrons and those in the Na^+ core, our MQC description of the Na_2 molecule in the gas phase gives good agreement with high-level quantum chemistry calculations[8,16], as summarized in Table 1. Figure 1a shows that the gas-phase Na_2 valence electron density forms a symmetric ovoid around the Na_2 centre of mass, as expected from the ideas of molecular-orbital theory[17,18]. When we insert the Na_2 molecule into solution, however, interactions between the solvent molecules and bonding electrons produce a

Department of Chemistry & Biochemistry, University of California, Los Angeles, Los Angeles, CA, USA. *e-mail: widmer@chem.ucla.edu; schwartz@chem.ucla.edu

Table 1 | Average bond length (r_e), vibrational frequency (ω_e) and instantaneous dipole moment ($\overline{\mu}$) for Na_2 in the gas phase and in various solution environments

System	r_e (Å)	ω_e (cm^{-1})	$\overline{\mu}$ (e-Å)
Gas phase exp[33–36]	3.08	159.1	0.0
Gas phase [CCSD(T)]	3.185 ± 0.004	149 ± 26	0.0
Gas phase [MQC]	3.270 ± 0.004	136 ± 23	0.0
Argon	3.167 ± 0.005	161 ± 48	0.11 ± 0.05
THF (average)	3.617 ± 0.002	112 ± 15	0.6 ± 0.4
$Na(THF)_3$–$Na(THF)_3$	3.472 ± 0.008	119 ± 33	0.4 ± 0.2
$Na(THF)_2$–$Na(THF)_4$	3.66 ± 0.01	108 ± 20	1.2 ± 0.3
$Na(THF)_3$–$Na(THF)_4$	3.692 ± 0.007	113 ± 24	0.7 ± 0.2

Values of r_e and ω_e for this work were obtained from harmonic fits to the well-bottom of the potential energy surface (gas phase) or potential of mean force (solution phase);see Fig. 4. The post-Hartree–Fock gas-phase fixed-point calculations were performed using coupled-cluster with singles, doubles and perturbative (linearized) triples [CCSD(T)] with the 6-311+G(*d*,*p*) basis set using GAUSSIAN 09. The gas-phase values calculated with our plane-wave-based CISD method give good agreement with theory at a similar level using more standard basis sets[16]. The quoted errors are standard deviations calculated from nonlinear least-squares fit.

valence electron density that is deformed relative to that in the gas phase. Figure 1b shows that when Na_2 is placed in liquid Ar, Pauli repulsion interactions from the surrounding cage of Ar atoms, on average, compress the solute's bonding electronic density, leading to a stiffer, tighter chemical bond (Table 1). As we saw previously[8], solvent fluctuations, even in apolar liquid Ar, induce relatively large instantaneous dipole moments, $\overline{\mu}$, on the solute (Table 1), even though the overall average dipole moment remains zero because the instantaneous dipoles point in random directions.

THF molecules, on the other hand, are known to chelate Na^+ in solution, with THF oxygen sites forming metal–oxygen dative bonds with a strength similar to that of a hydrogen bond (about 5 kcal mol^{-1}). We have shown previously on the basis of both MQC simulations and ultrafast spectroscopy experiments that when bare Na atoms are created in liquid THF, THF molecules push the Na valence electron off-centre to allow for the formation of Na–THF oxygen site dative bonds. In other words, the neutral atomic Na species in liquid THF is best thought of as a Na^+–solvated electron tight-contact pair rather than a solvated atom[13,19]. Indeed, when simulated with the same potentials and methods used in the current study[13,19], the calculated properties of sodium cation:electron contact pairs were found to be in excellent agreement with experiment[20,21]. Unlike what happens with bare Na atoms, the Na_2 molecule simulated here remains intact in liquid THF, but Fig. 1c shows that, similar to the Na^+–solvated electron tight-contact pair, local interactions with the solvent displace the solute valence electron density to expose part of each Na^+ core for chelation by the THF oxygen sites. The net effect of these dative interactions with the solvent is to cause the solute valence electron density to spill out away from the bond axis, leading to instantaneous dipole moments that are much larger than in liquid Ar. Also in contrast to the bond compression seen in liquid Ar, the THF–Na^+ interactions lead to a large increase in the Na–Na bond length (Table 1).

To better understand the local interactions between Na_2 and THF, the black curve in Fig. 2 shows the Na^+–THF oxygen site radial distribution function, $g(r)$, averaged over both Na^+ cores. The large peak at 2.35 Å that dominates the $g(r)$ corresponds to THF oxygen sites that coordinate the Na^+ core; this dative bond distance is the same as that for solvation of both bare Na^+ ions and Na^+–solvated electron tight-contact pairs in liquid THF[13,22]. Although six THF molecules coordinate a bare Na^+, and four coordinate the neutral Na species[13], integration of the $g(r)$ for Na_2 in THF reveals an average coordination of 3.25 THF oxygen atoms making dative bonds per Na cation.

To understand why the average coordination number is not an integer and why the THF-solvated Na–Na bond length is longer than that in the gas phase or liquid Ar, we examined the free energies involved in THF coordination of Na_2. To do this, we introduce a continuous coordination number, n_{Na^+}, defined as the number of THF oxygen sites that reside within a certain distance of the atomic centre (actually, the integrated number of THF oxygens weighted by the function $S(r)$, shown as the dashed green curve in Fig. 2; this is very similar to the coordinate we used in our previous work on Na^+–solvated electron tight-contact pairs in liquid THF, and details are provided in the Methods). By examining the distribution of n_{Na^+} along our equilibrium Na_2/THF trajectory, we were able to calculate the free energy A, or potential of mean force (PMF), as a function of the coordination number coordinate for each Na atom (Fig. 3a). The figure shows clearly that there are only a few stable Na_2 coordination states, and that the minima in A occur precisely at integer coordination numbers. The coordination states accessible at equilibrium are $Na(THF)_3$–$Na(THF)_3$, $Na(THF)_2$–$Na(THF)_4$ and $Na(THF)_3$–$Na(THF)_4$ (referred to as (3,3), (2,4) and (3,4) in the figures), which occur at room temperature with relative populations of roughly 50:17:54, respectively, explaining the average THF coordination number of 3.25. The figure also shows that these stable coordination states interconvert along pathways where n_{Na^+} on one Na^+ core remains fixed while the other Na^+ core either gains or loses a single coordinating THF.

Figure 3b,c also shows one-dimensional slices along two of the coordination-state conversion pathways, revealing relatively large potential energy barriers (~8 k_BT high) that must be overcome to convert between coordination states. Indeed, we see that at equilibrium the typical interconversion time at room temperature for the $Na(THF)_3$–$Na(THF)_4 \rightarrow Na(THF)_3$–$Na(THF)_3$ reaction is ~37 ps, and ~32 ps for the reverse $Na(THF)_3$–$Na(THF)_3 \rightarrow Na(THF)_3$–$Na(THF)_4$ interconversion reaction. We also see an ~38 ps conversion time for the $Na(THF)_3$–$Na(THF)_4 \rightarrow Na(THF)_2$–$Na(THF)_4$ reaction and ~16 ps for the reverse $Na(THF)_2$–$Na(THF)_4 \rightarrow Na(THF)_3$–$Na(THF)_4$ reaction (see Supplementary Section 'Coordination Number Interconversion' for details). These 'reaction times' observed during the simulation trajectory match quite well with values predicted from transition state theory, as shown in the Supplementary Information, consistent with the assignment of the interconversion between coordination states as chemical reactions. Clearly, the coordination states at each free energy minimum can be thought of as distinct chemical species, with reactive pathways connecting the different species in equilibrium. Thus, even though each Na^+–THF dative bond has a strength that is similar only to that of a hydrogen bond, the collective interaction of the solute with the solvent produces a variety of new chemical species that are in equilibrium, each of which is distinguished only by the involvement of the solvent.

To verify that the solvent-induced changes in molecular identity we see make sense, we used density functional theory (DFT) to calculate the relative energies of the different Na_2/THF coordination states extracted from our MQC simulations, performing calculations on geometry-optimized configurations from our simulations extracted at both the free energy minima and at the tops of the interconversion barriers. Because the coordination states involve relatively weak dative interactions between the THF oxygen and sodium atoms, we used the range-separated hybrid ωB97M-V functional, which includes non-local correlation[23]; the details of how we performed these fixed-point calculations are provided in the Supplementary Section 'Verification of Results with DFT Calculations'. Indeed, we find, as summarized by the black asterisks in Fig. 3b,c, that the relative energetics calculated both directly in the MQC simulations and by DFT, for both the different coordination states and the barriers for their interconversion, agree to within one or two k_BT, an amount that is well within the error of the DFT calculations.

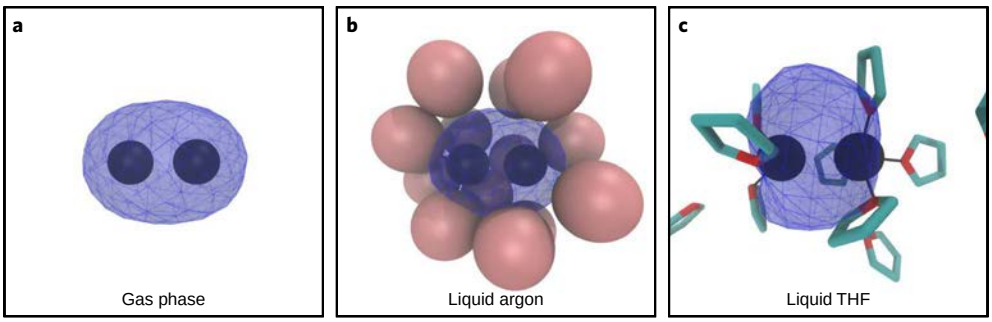

Fig. 1 | Representative simulation snapshots of Na_2 reveal deformation of the bonding electronic density in the condensed phase. a–c, Na^+ cores are plotted as black spheres (scaled to their ionic radius) and valence electrons are represented as a transparent blue surface with a blue wire mesh, enclosing 90% of the charge density. The first solvation shell of Ar atoms (with a cutout to enable viewing of the electron density) are plotted as pink spheres (scaled to their van der Waals radius), and THF molecules are plotted as light blue sticks with red oxygen atoms. Dative bonds between Na^+ and THF oxygen sites within 3.5 Å are drawn with thin black lines. For the sodium dimer in THF, the snapshot shown is for the most commonly occurring $Na(THF)_3$–$Na(THF)_4$ coordination state. Representative snapshots for other coordination states and further discussion are provided in Supplementary Figs. 6–8. In the gas phase (**a**) the bonding electron density forms a symmetric ovoid around the dimer centre of mass. However, in liquid argon (**b**) the electron density is compressed, resulting in a slightly shorter average bond length. In liquid THF (**c**) the Na^+–THF oxygen site dative bonds elongate the Na_2 bond length and distort the electron density.

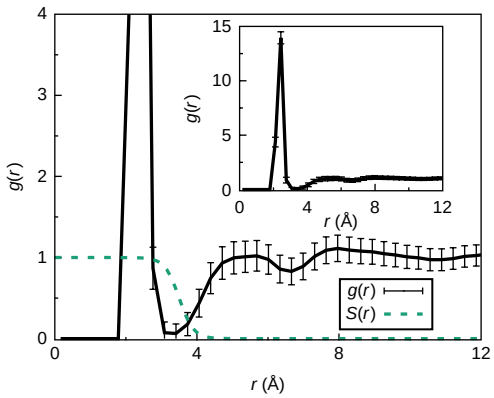

Fig. 2 | Pair distribution function *g*(*r*), showing chelation of the Na^+ cores in Na_2 by THF, leading to the formation of metal–oxygen dative bonds. *g*(*r*) is averaged over Na^+–THF oxygen site distances for both Na^+ cores. The dashed green curve shows the smooth weighting function, *S*(*r*), used to define the THF coordination number around the Na^+ cores. Inset: *g*(*r*) on an expanded scale, revealing the full coordination of the Na^+ cores by THF molecules at the 2.35 Å dative bond distance. Error bars represent 95% confidence intervals. The sharp coordination peak at 2.35 Å, similar to that observed for the Na^+–solvated electron tight-contact pairs formed from bare sodium in liquid THF, reveals that THF molecules displace the Na_2 bonding electron density, exposing both Na^+ cores for chelation.

How unique are the Na_2 chemical species that differ only in their local coordination with the solvent? In Fig. 4 we compare the potential energy of the gas-phase Na_2 molecule (black curve) to the PMF for the molecule in liquid Ar (orange curve), in liquid THF on average (purple dotted curve) and for each of the stable THF-solvated coordination states (red, green and blue curves) as a function of the Na–Na bond distance. These are the potential energy surfaces that govern how the two Na atoms move in each of the respective environments. The figure shows clearly that the overall PMF for the sodium dimer in liquid THF is not smooth; there are wiggles at the bottom of the well that result from the presence of the different (and distinct) solvent coordination states. Thus, it makes much more sense to think of the Na_2/THF system as three different molecules in equilibrium. As summarized in Table 1, each THF coordination state has a different Na–Na bond length (r_e, the position of the minimum in the PMF) and a different vibrational frequency (ω_e, the curvature of the PMF around the minimum), verifying that each is a unique chemical species.

Figure 5a shows the vibrational motions of Na_2 in the different environments, calculated as power spectra (Fourier transforms) of the bond velocity autocorrelation function, $C(t) = \langle v(t) \cdot v(0) \rangle$ (see Supplementary Section 'Simulated Spectra Calculations' for details). The peak in the power spectrum in liquid Ar is blueshifted from that in the gas phase because, on average, Pauli repulsion interactions from the first-shell Ar solvent molecules compress the bonding electrons and shorten the overall bond length, thus raising the Na_2 vibrational frequency[8]. In liquid THF, however, the main Na–Na vibrational peak is lowered in frequency; the purple dotted curve shows that, on average, the Na atom motions in THF occur at a frequency more than 10 cm^{-1} below that predicted by the curvature of the average PMF for the dimer in THF (Table 1). However, the frequencies of the lowered Na–Na vibrational motions in THF match nearly perfectly those predicted by the curvatures of the individual coordination-state PMFs in (cf. Fig. 4 and Table 1). Figure 5a also shows the presence of a sharper blueshifted peak near ~200 cm^{-1} that is nearly double that of the gas-phase vibrational frequency. This higher-frequency motion corresponds to the stretching of the Na^+–THF oxygen dative bonds, as verified by tracking the bond velocities of the dative bonds during intervals where the dimer remained in a single coordination state. Like the Na–Na vibrational peak, the dative bond stretching peak shifts with coordination number, with less-coordinated Na^+ cores holding the datively bound THFs more tightly, resulting in a slightly higher stretching frequency. This also explains the splitting of the high-frequency peak for the asymmetrically coordinated states, which have two types of solvent dative bonding interaction in a single molecule. The net result is that the Na atoms move at multiple new frequencies when the dimer is placed in liquid THF, and these frequencies can only be clearly resolved by considering the individual solvent-controlled coordination states.

In liquid Ar, we showed previously that solvent collisions push the bonding electrons in Na_2 off-centre, creating randomly oriented instantaneous dipole moments for the non-polar molecule in the non-polar solvent that produce an infrared absorption spectrum[8]. In liquid THF, we see in Table 1 that the symmetrically coordinated $Na(THF)_3$–$Na(THF)_3$ species behaves similarly to that in liquid Ar, although the average value of the instantaneous dipole is somewhat larger in THF. However, for the asymmetrically coordinated

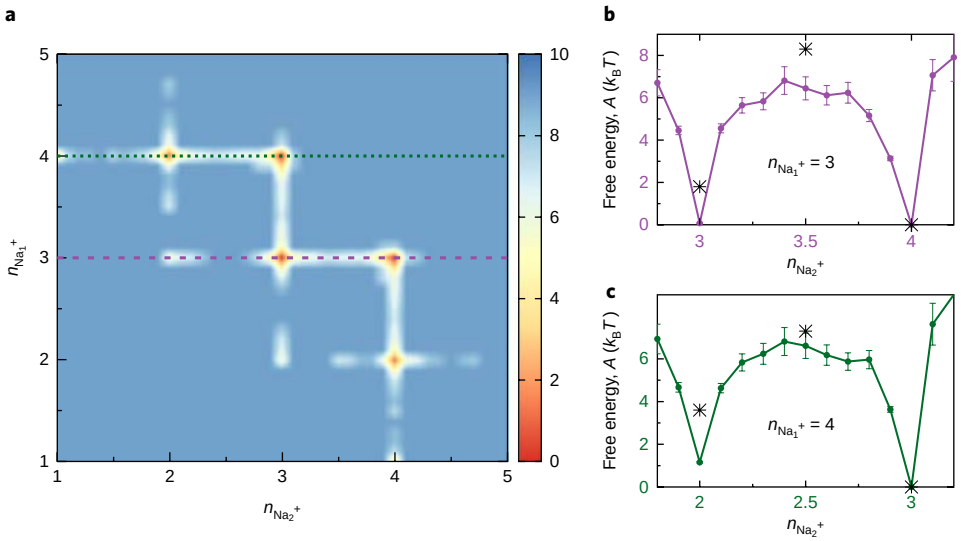

Fig. 3 | The stable coordination states of Na_2 in liquid THF behave as distinct molecules. a, PMF as a function of the Na^+–THF solvent coordinate, n_{Na^+} (generated by summing the number of THF oxygen atoms weighted by $S(r)$ in Fig. 2), for each Na^+ core. The data clearly reveal multiple stable states with integer numbers of coordinated THF molecules that are connected by conversion pathways in which the coordination of one Na^+ core changes by a single THF molecule. **b**,**c**, Slices along the $n_{Na_1^+}=3$ (**b**) and the $n_{Na_1^+}=4$ (**c**) conversion pathways reveal steep potential barriers of several k_BT that must be overcome to convert between the stable coordination states, like the energy barriers of a traditional chemical reaction coordinate. Error bars represent 95% confidence intervals. For comparison, the results of fixed-point DFT calculations (see Supplementary Section 'Verification of Results with DFT Calculations' for details) using the range-separated hybrid ωB97M-V functional[23] with implicit solvent are shown as black asterisks.

chelation states, the average net displacement of the Na_2 bonding electronic density from the more-coordinated to the less-coordinated Na^+ core gives rise to a permanent dipole. Thus, even though gas-phase Na_2 has no dipole and is completely infrared inactive, in solution the molecule should be at least weakly infrared active, and should have an even stronger infrared absorption for chemical species such as $Na(THF)_2$–$Na(THF)_4$ and $Na(THF)_3$–$Na(THF)_4$ that have permanent dipole moments.

Figure 5b shows the calculated infrared spectra (Fourier transform of the dipole autocorrelation function; see Supplementary Section 'Simulated Spectra Calculations') of Na_2 in each of the various environments considered here. Each spectrum shows a large peak at low frequencies (~50 cm^{-1} in Ar and ~20 cm^{-1} in THF), resulting from intermolecular rattling motions of the entire coordinated dimer species in the cage of surrounding solvent molecules, a motion that strongly modulates the molecular dipole moment[8,24]. In THF, the infrared spectrum of each coordination state also shows a peak at ~200 cm^{-1}, the stretching frequency of the Na^+–THF oxygen site dative bonds; as the dative bonds become slightly shorter or longer, this pushes (or pulls) the bonding electron density away from (or towards) the Na–Na internuclear space, modulating the overall solute dipole moment. Furthermore, each of the chelated species in THF shows a shoulder in their infrared spectrum at ~60 cm^{-1}, which is the vibrational frequency of the fully chelated Na atoms (including their coordinated solvent molecules) moving against each other, also modulating the overall dipole moment. This shoulder does not appear when considering the overall infrared spectrum for the dimer in THF (purple dotted curve), indicating that the modulation of the dipole of the sodium dimer in THF cannot be explained without isolating the behaviour of the specific individual coordination states.

Not only do the different Na_2 solvent coordination states have different vibrational spectra, they also have different predicted electronic absorptivity. Figure 5c shows the calculated UV–visible absorption spectra for Na_2-based species in different environments. Details of how we calculated the spectra are provided in the Supplementary Section 'Simulated Spectra Calculations' but are similar to those in our previous work[8,12,19]. In apolar liquid Ar, the electronic absorption spectrum resembles that in the gas phase, although it is somewhat blueshifted, as expected because the valence electrons in Ar are more compressed than in the gas phase. In liquid THF, however, the absorption spectra of the different coordination

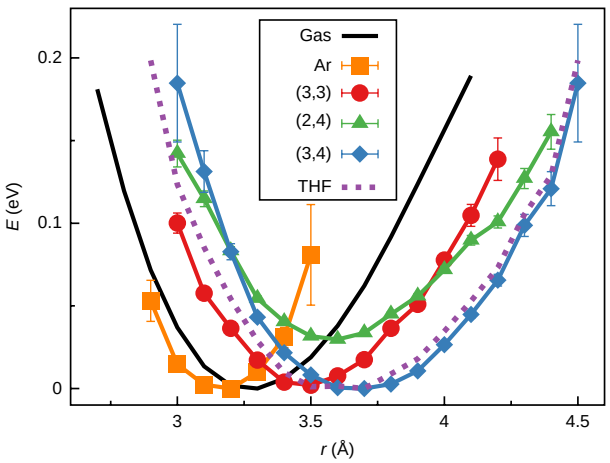

Fig. 4 | Different potentials of mean force for the Na_2 molecule with different local solvent coordination in liquid THF. The gas-phase potential energy surface for Na_2, calculated with our MQC model (as described in ref. [8]), is plotted in black with the minimum set to zero. The PMFs for each Na_2 coordination state in liquid THF are plotted using the different coordination state energies seen in Fig. 3 to illustrate the relative probabilities. The overall PMF in liquid THF (purple dotted line) is not smooth, most notably with wiggles present in the curve bottom, even though the statistics are more than enough to preclude noise at this level. In contrast, the PMFs of the individual coordination states are quite smooth, highlighting the necessity of thinking of the Na_2/THF system as three discrete molecules in equilibrium rather than an overall average. Error bars represent 95% confidence intervals.

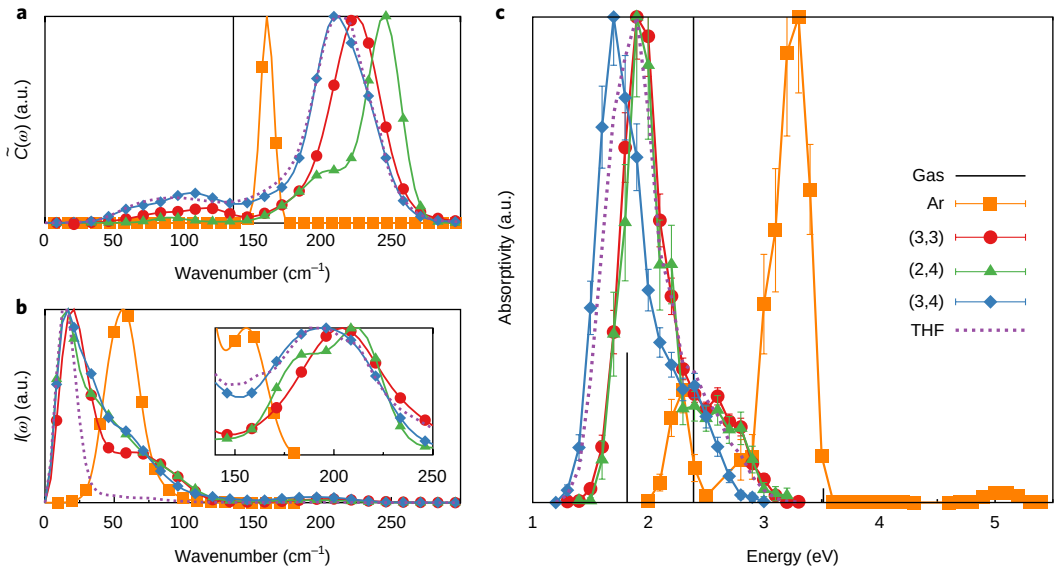

Fig. 5 | Different Na_2 coordination states are spectroscopically distinct. a, Vibrational spectra of Na_2 calculated from the Fourier transform of the bond velocity autocorrelation function. The gas-phase vibrational frequency is shown as a black line at 136 cm^{-1}. The vibrational spectrum in liquid Ar (orange curve) is blueshifted relative to the gas phase, as expected from compression of the Na_2 bonding electrons due to Pauli repulsion interactions with the first-shell Ar solvent molecules. In liquid THF (purple dotted curve for the overall coordination states; blue, green and red curves for the individual states), however, the main Na–Na vibrational peak is redshifted due to elongation of the bond with a second, sharper peak near 200 cm^{-1} from the motions of the Na^+–THF oxygen dative bonds. **b**, Infrared spectra of Na_2 in different solution environments calculated as the Fourier transform of the dipole moment autocorrelation function; the molecule has no infrared spectrum in the gas phase. In addition to the large peak at ~50 cm^{-1} in Ar and ~20 cm^{-1} in THF (due to intermolecular rattling motions in the solvent cage), features of the dipole motion modulation are present at ~60 cm^{-1} for the different THF coordination states (vibration of the fully chelated sodium atoms), ~160 cm^{-1} for Na_2 in Ar (Na_2 intramolecular vibration) and ~200 cm^{-1} for Na_2 in THF (dative bond vibration(s)). **c**, Calculated electronic absorption spectra for the Na_2 molecule in different environments. The gas-phase absorbance is plotted as vertical black lines scaled by their relative oscillator strengths. Similar to the vibrational spectra, the Na_2 electronic absorption spectrum is blueshifted in liquid Ar but redshifted in liquid THF. The average electronic spectrum in THF is not interpretable unless decomposed into spectra of the individual coordination states. Error bars represent 95% confidence intervals.

states are predicted to redshift relative to the gas phase due to the elongation of the Na_2 bond and displacement of electron density away from the Na^+ cores. The magnitude of the redshift increases with increasing coordination. The $Na(THF)_2$–$Na(THF)_4$ and $Na(THF)_3$–$Na(THF)_3$ states, each with a total coordination number of 6, shift ~0.4 eV to the red of the gas-phase maximum, while the $Na(THF)_3$–$Na(THF)_4$ state, with a total coordination number of 7, shifts nearly twice as much. It is worth noting that if one were to ignore the existence of the different coordination states and examine only the average absorption spectrum of Na_2 in THF (purple dotted curve), the main peak would have an unusually broad width, and the presence of the secondary peak due to transitions to higher excited states would be lost, potentially leading to a mis-assignment of the observed spectral features.

Finally, we note that even though these predictions of solvent control over molecular identity have been made on the basis of computer simulations, it should be possible to verify all of these predictions experimentally. Solvated Na_2 molecules have already been prepared in low-temperature rare gas matrices by co-evaporating Na metal with the solvent, and the Raman spectrum of the solvated dimers has been measured[25–31]. It should be feasible to create Na_2 in other good evaporatable glass-forming liquids, such as 2-methyl-THF[32], which ought to show all the same distinct infrared and UV–visible spectroscopic features predicted here for unsubstituted THF. Moreover, if there is some way to prepare Na_2 transiently at room temperature, our simulations suggest that the different chelated species interconvert on a timescale slow compared to the vibration timescale, so that ultrafast spectroscopy techniques should be able to test our predictions. Furthermore, we have performed preliminary simulations of the sodium dimer cation (Na_2^+) in liquid THF, and found that there are similar coordination states, although with slightly higher average coordination numbers. This opens the possibility for preparing mass-selected gas-phase Na_2^+/THF clusters, whose spectroscopy and properties could also be probed directly. Whether prepared as neutral dimers or molecular cations, it should be possible to experimentally confirm the presence of the different solvent-coordinated chemical species in equilibrium by vibrational or electronic spectroscopy.

Conclusions

In summary, MQC MD simulations of Na_2 in liquid THF reveal that the solvent plays an intimate role in the bond dynamics, electronic properties and, indeed, chemical identity of simple solutes. Even though there are only relatively weak local specific interactions between Na atoms and liquid THF, we find that several unique coordination states of Na_2 are stable under equilibrium conditions: $Na(THF)_2$–$Na(THF)_4$, $Na(THF)_3$–$Na(THF)_3$ and $Na(THF)_3$–$Na(THF)_4$. There is no simple way to explain the average properties of Na_2 in THF except by thinking of each coordination state as a different molecule that undergoes a series of equilibrium chemical reactions, crossing free energy barriers of ~8 k_BT to convert from one stable coordination state to another. Indeed, the rates at which the different coordination states interconvert are consistent with simple transition state theory, adding credence to their identity as separate chemical species. Moreover, each coordination species has a unique bond length, distinct bond dynamics and different infrared and UV–visible absorption spectra, providing an experimental handle to test the idea that interactions with the solvent can induce changes in solute chemical identity. We close by reiterating that the local specific interactions responsible for this behaviour, the formation of Na–THF

oxygen dative bonds, are no stronger than the hydrogen bonds that help form the secondary structure of peptides and proteins or lead to clathrate formation in aqueous solutions. This suggests that the concept of solvent participation in chemical identity, with chemical reactions converting between different local coordination states, is likely ubiquitous throughout solution chemistry and biochemistry.

Methods

Overview of simulation details. Our MQC MD simulations consisted of classical solvent molecules, two classical Na^+ cations and two fully quantum mechanical electrons. Interactions between the classical particles and the quantum mechanical electrons were accounted for using Phillips Kleinmen (PK) pseudopotentials[37], modified with polarization potentials to correct for the frozen-core approximation implicit in PK formalism[11,38,39]. An overview of the classical interactions and pseudopotentials used is provided in the Supplementary Section 'Mixed/Quantum Classical Model' as well as in our previous work[10–13]. Simulations in liquid Ar involved 1,600 solvent molecules in a cubic simulation cell of side length 43.8 Å, while those in liquid THF used 254 solvent molecules contained in a cubic simulation cell with side length 32.5 Å. The simulation cell lengths were chosen to match the experimental solvent densities at the simulation temperature (1.26 g ml^{-1} at 120 K for the Ar simulations and 0.89 g ml^{-1} at 298 K for the THF simulations). Periodic boundary conditions were implemented with minimum image convention[40] and all interactions were tapered smoothly to zero at 16 Å over a 2 Å range using a centre-of-mass-based switching function according to Steinhauser[41].

We used our two-electron Fourier grid (2EFG) electronic structure algorithm[9] to solve the time-independent Schrödinger equation for the electrons' wavefunction at every time step (5 fs in Ar and 4 fs in THF). The valence electrons' eigenstates were expanded on a six-dimensional real-space grid. For Ar, we used a basis of $16\times16\times16$ grid points spread over a 14 Å^3 box, and for THF we used a basis of $20\times20\times20$ grid points dispersed over a 17.5 Å^3 box, for a consistent grid spacing of 0.875 Å. These dimensions were chosen to keep the basis set as small as possible for each system while still capturing both the spatial extent and the solvent-induced distortions of electronic wavefunction. We centred the grid in the middle of the simulation cell and shifted all classical particles relative to the grid every 500 fs to avoid leakage of the wavefunction at the edges of the grid basis and so that the wavefunction was always located roughly in the centre of the simulation cell. The classical particles were shifted an integer number of grid spaces to avoid discontinuities in the quantum energy that would prevent the total energy of simulation from being conserved. The Ar simulation was equilibrated at 120 K (within the liquid region of the phase diagram)[17,42] and the THF simulation at 298 K before 500 ps production trajectories were run.

Definition of coordination coordinate. To develop the coordination coordinate used to construct our coordination PMF, we first defined a continuous coordination number variable, n_{Na^+}, as

$$n_{Na^+} = \sum_i S(|r_{O,i} - r_{Na^+}|) \quad (1)$$

where i runs over every THF oxygen site and r_{Na^+} and $r_{O,i}$ are the positions of the Na^+ core and the ith oxygen site respectively. The Fermi function $S(r)$ is defined as $S(r) = \frac{1}{\exp[\kappa(r - r_c)] + 1}$, where r_c is a cutoff radius that defines when a solvent molecule is coordinated to the Na^+, and κ^{-1} is the width of the transition region where the Fermi function switches from 1 to 0 around r_c. For this work, we selected $\kappa^{-1} = 0.2$ Å and $r_c = 3.50$ Å, corresponding to the first minimum of the Na^+–THF oxygen site $g(r)$. These values are similar to those used by our group for studies of sodium neutral in THF[13] but have been re-optimized for the Na_2 molecule. Equation (1) was evaluated for each Na^+ core to generate the plots in Fig. 3.

PMF calculations. All PMF plots for coordination number were calculated based on the negative natural logarithm of the occurrence probabilities of each state. First, we binned up the number of production run configurations in each state, assuming Poisson statistics such that the error for each bin count was simply its square root. Next, we normalized the histogram results by dividing by the maximum bin count. Finally, we generated the PMF free energy values, A, in k_BT by taking the negative natural logarithm of the normalized bin counts. The normalization ensured that the most probable state is plotted at $0\,k_BT$. The free energy error was propagated according to $\sigma = \pm\frac{\sqrt{\text{bincount}}/\text{maxbincount}}{\text{bincount}/\text{maxbincount}}$. Because the proportion of configurations in each Na_2 coordination state accessed at equilibrium in THF are of similar amounts, we did not need to use umbrella sampling to improve the statistics (the relative population values for the $Na(THF)_3$–$Na(THF)_3$, $Na(THF)_2$–$Na(THF)_4$,and $Na(THF)_3$–$Na(THF)_4$ were 50:17:54, respectively). We note that in our previous work on the related sodium cation–solvated electron contact pair, direct sampling of the different coordination states was in excellent agreement with those determined by importance sampling[19].

Data availability. Any data generated and analysed for this study that are not included in this Article and its Supplementary Information are available from the authors upon reasonable request.

Code availability. The computer code used in this study is available from the authors upon reasonable request.

Received: 13 October 2017; Accepted: 13 April 2018;
Published online: 21 May 2018

References

1. Young, R. M. & Neumark, D. M. Dynamics of solvated electrons in clusters. *Chem. Rev.* **112**, 5553–5577 (2012).
2. Blandamer, M. J. & Fox, M. F. Theory and applications of charge-transfer to solvent spectra. *Chem. Rev.* **70**, 59–93 (1970).
3. Marcus, R. A. On the theory of oxidation–reduction reactions involving electron transfer. 1. *J. Chem. Phys.* **24**, 966–978 (1956).
4. Marcus, R. A. & Sutin, N. Electron transfers in chemistry and biology. *Acta Biochim. Biophys.* **811**, 265–322 (1985).
5. Barthel, E. R., Martini, I. B. & Schwartz, B. J. How does the solvent control electron transfer? Experimental and theoretical studies of the simplest charge transfer reaction. *J. Phys. Chem. B.* **105**, 12230–12241 (2001).
6. Suppan, P. Solvatochromic shifts: the influence of the medium on the energy of electronic states. *J. Photochem. Photobiol.* **50**, 293–330 (1990).
7. Bagchi, B. Isomerization dynamics in solution. *Int. Rev. Phys. Chem.* **6**, 1–33 (1987).
8. Glover, W. J., Larsen, R. E. & Schwartz, B. J. How does a solvent affect chemical bonds? Mixed quantum/classical simulations with a full CI treatment of the bonding electrons. *J. Phys. Chem. Lett.* **1**, 165–169 (2010).
9. Glover, W. J., Larsen, R. E. & Schwartz, B. J. First principles multi-electron mixed quantum/classical simulations in the condensed phase. I. An efficient Fourier-grid method for solving the many-electron problem. *J. Chem. Phys.* **132**, 144101 (2010).
10. Glover, W. J., Larsen, R. E. & Schwartz, B. J. The roles of electronic exchange and correlation in charge-transfer-to-solvent dynamics: many-electron non-adiabatic mixed quantum/classical simulations of photoexcited sodium anions in the condensed phase. *J. Chem. Phys.* **129**, 1–20 (2008).
11. Smallwood, C. J., Mejia, C. N., Glover, W. R., Larsen, R. E. & Schwartz, B. J. A computationally-efficient exact pseudopotential method. 2. Application to the molecular pseudopotential of an excess electron interacting with tetrahydrofuran (THF). *J. Chem. Phys.* **125**, 9681–9691 (2006).
12. Glover, W. J., Larsen, R. E. & Schwartz, B. J. First principles multi-electron mixed quantum/classical simulations in the condensed phase. II. The charge-transfer-to-solvent states of sodium anions in liquid tetrahydrofuran. *J. Chem. Phys.* **132**, 144102 (2010).
13. Glover, W. J., Larsen, R. E. & Schwartz, B. J. The nature of sodium atoms/(Na^+–e^-) contact pairs in liquid tetrahydrofuran. *J. Phys. Chem. B* **114**, 11535–11543 (2010).
14. Gervais, B. et al. Simple DFT model of clusters embedded in rare gas matrix: trapping sites and spectroscopic properties of Na embedded in Ar. *J. Chem. Phys.* **121**, 8466–8480 (2004).
15. Szaz, L. *Pseudopotential Theory of Atoms and Molecules*. (Wiley: New York, 1985).
16. Liu, Z., Carter, L. E. & Carter, E. A. Full configuration interaction molecular dynamics of Na_2 and Na_3. *J. Phys. Chem.* **99**, 4355–4359 (1995).
17. Lennard-Jones, J. E. The electronic structure of some diatomic molecules. *Trans. Faraday Soc.* **25**, 668–686 (1929).
18. Coulson, C. A. Representation of simple molecules by molecular orbitals. *Q. Rev. Chem. Soc.* **1**, 144–178 (1947).
19. Glover, W. J., Larsen, R. E. & Schwartz, B. J. Simulating the formation of sodium:electron tight-contact pairs: watching the solvation of atoms in liquids one molecule at a time. *J. Phys. Chem. A* **115**, 5887–5894 (2011).
20. Bragg, A. E., Glover, W. J. & Schwartz, B. J. Watching the solvation of atoms in liquids one solvent molecule at a time. *Phys. Rev. Lett.* **104**, 233005 (2010).
21. Cavanagh, M. C., Larsen, R. E. & Schwartz, B. J. Watching Na atoms solvate into Na^+–e^- contact pairs: untangling the ultrafast charge-transfer-to-solvent dynamics of Na^- in tetrahydrofuran (THF). *J. Phys. Chem.* **111**, 5144–5157 (2007).
22. Chandrasekhar, J. & Jorgensen, W. L. The nature of dilute-solutions of sodium-ion in water, methanol, and tetrahydrofuran. *J. Chem. Phys.* **77**, 5080–5089 (1982).
23. Mardirossian, N. & Head-Gordon, M. ωB97M-V: a combinatorially optimized, range-separated hybrid, meta-GGA density functional with VV10 nonlocal correlation. *J. Chem. Phys.* **144**, 214110–214200 (2016).
24. Bedard-Hearn, M. J., Larsen, R. E. & Schwartz, B. J. Understanding nonequilibrium solvent motions through molecular projections: computer simulations of solvation dynamics in liquid tetrahydrofuran (THF). *J. Phys. Chem. B* **107**, 14464–14475 (2003).
25. Kornath, A., Zoermer, A. & Ludwig, R. Formation of the magic cluster Na_8 in noble gas matrixes. *Inorg. Chem.* **41**, 6206–6210 (2002).

26. Kornath, A., Ludwig, R. & Zoermer, A. Small potassium clusters. *Angew. Chem. Int. Ed.* **37**, 1575–1577 (1998).
27. Ozin, G. A. & Huber, H. The matrix optical spectra of sodium molecules containing from two to four atoms. *Inorg. Chem.* **18**, 1402–1406 (1979).
28. Welker, T. & Martin, T. P. Optical-absorption of matrix isolated Li, Na, and Ag clusters and microcrystals. *J. Chem. Phys.* **70**, 5683–5691 (1979).
29. Hofmann, M., Leutwyler, S. & Schulze, W. Matrix isolation-aggregation of sodium atoms and molecules formed in a supersonic nozzle bean. *Chem. Phys.* **40**, 145–152 (1979).
30. Froben, F. W. & Schulze, W. Raman measurements of matrix-isolated small metal-clusters. *Phys. Chem. Chem. Phys.* **88**, 312–314 (1984).
31. Kornath, A., Zoermer, A. & Ludwig, R. Raman spectroscopy investigation of matrix-isolated rubidium and cesium molecules: Rb_2, Rb_3, Cs_2, and Cs_3. *Inorg. Chem.* **38**, 4696–4699 (1999).
32. Scott, D. R. & Allison, J. B. Solvent glasses for low temperature spectroscopic studies. *J. Phys. Chem.* **66**, 561–562 (1962).
33. Kato, H., Matsui, T. & Noda, C. Na_2 ($A^1\sum^+_u \rightarrow X^1\sum^+_g$) fluorescence accompanied by a continuous spectrum. *J. Chem. Phys.* **76**, 5678–5683 (1982).
34. Verma, K. K., Bahns, J. T., Rajeiriza, A. R., Stwalley, W. C. & Zemke, W. T. First observation of bound-continuum transitions in the laser-induced $A^1\sum^+_u \rightarrow X^1\sum^+_g$ fluorescence of Na_2. *J. Chem. Phys.* **78**, 3599–3613 (1983).
35. Barrow, R. F., Verges, J., Eff ntin, C., Hussein, K. & D'incan, J. Long-range potentials for the $X^1\sum^+_g$ and $(1)^1\sum_g$ states and the dissociation energy of Na_2. *Chem. Phys. Lett.* **104**, 179–183 (1984).
36. Babaky, O. & Hussein, K. The ground state $X^1\sum^+_g$ of Na_2. *Can. J. Phys.* **67**, 912–918 (1989).
37. Phillips, J. C. & Kleinman, L. New method for calculating wave functions in crystals and molecules. *Phys. Rev.* **116**, 287–294 (1959).
38. Smallwood, C. J., Larsen, R. E., Glover, W. G. & Schwartz, B. J. A computationally-effici t exact pseudopotential method. I. Analytic reformulation of the Philips–Kleinman theory. *J. Chem. Phys.* **125**, 074102 (2006).
39. Larsen, R. E., Glover, W. J. & Schwartz, B. J. Does the hydrated electron occupy a cavity? *Science* **329**, 65–69 (2010).
40. Allen, M. P. & Tildesley, D. J. *Computer Simulation of Liquids* (Oxford Univ. Press, London, 1992).
41. Steinhauser, O. Reaction fi ld simulation of water. *Mol. Phys.* **45**, 335–348 (1982).
42. Smit, B. Phase-diagrams of Lennard-Jones fluids. *J. Chem. Phys.* **96**, 8639–4860 (1992).

Acknowledgements

Early portions of this work were supported by the National Science Foundation (grant CHE-1565434). Beginning in September 2017, this work was supported by the US Department of Energy Condensed Phase and Interfacial Molecular Science programme (grant 0000228903). The authors acknowledge the Institute for Digital Research and Education (IDRE) at UCLA for use of the hoffman2 computing cluster, B. Taggart for assistance setting up the simulations, and W. Glover and C.-C. Zhou for discussions.

Author contributions

The work described in this text was completed by D.R.W. under the supervision of B.J.S.

Competing interests

The authors declare no competing interests.

Additional information

Supplementary information is available for this paper at https://doi.org/10.1038/s41557-018-0066-z.

Reprints and permissions information is available at www.nature.com/reprints.

Correspondence and requests for materials should be addressed to D.R.W. or B.J.S.

Publisher's note: Springer Nature remains neutral with regard to jurisdictional claims in published maps and institutional affiliations.